

Enhanced Field-Oriented Control for Synchronous Reluctance Motors Using Fuzzy Logic

Sayed O. Madbouly

Department of Electrical Engineering, College of Engineering, Qassim University, Saudi Arabia.

Article Info

Article history:

Received Nov 22, 2024

Revised Feb 24, 2025

Accepted Mar 2, 2025

Keywords:

Fuzzy logic
Field oriented control
Electrical drives
Energy conversion
machines

ABSTRACT

This paper presents a fuzzy logic-based Field Oriented Control (FOC) strategy for synchronous reluctance motors (SynRMs). The proposed algorithm addresses the inherent nonlinearities and parameter sensitivities of SynRMs by integrating fuzzy logic control (FLC) into the FOC framework, enhancing system robustness and adaptability. The SynRM model is derived in the rotor reference frame, with two control loops implemented: one for speed control and the other for flux control. Two FLCs are utilized in the speed control loop, while one FLC is adopted in the flux control loop. Fuzzy sets, membership functions, and rule bases enable dynamic parameter tuning. The entire system is simulated in MATLAB/Simulink. The system's dynamic performance is rigorously evaluated in two scenarios: with decoupling control components between the speed and flux control loops, and without these components under various loading conditions. Comprehensive simulations demonstrate that the proposed control algorithm, without decoupling control components, exhibits superior dynamic performance in terms of rise time, overshoot, and settling time. Furthermore, eliminating the decoupling components reduces the system's dependency on machine parameters while having a minor effect on undershoot.

Copyright © 2025 Institute of Advanced Engineering and Science.
All rights reserved.

Corresponding Author:

Sayed O. Madbouly,
Department of Electrical Engineering,
College of Engineering,
Qassim University, Saudi Arabia.

Email: so.ossman@qu.edu.sa, sayed_madpouly@hotmail.com

1. INTRODUCTION

Recently, the demand for high-efficiency, cost-effective electric motors has driven significant advancements in motor technology [1]. Driven by the demand for sustainable energy and improved industrial efficiency, synchronous reluctance motors (SynRMs) have emerged as a promising alternative to permanent magnet synchronous motors (PMSMs) and induction motors, offering advantages such as simplicity, robustness, and high efficiency under diverse operating conditions [2-6].

Synchronous reluctance motors operate on the principle of reluctance torque, which is generated as the rotor aligns with the stator magnetic field to minimize magnetic reluctance [7]. The rotor lacks windings or permanent magnets, instead featuring a laminated iron core with air gaps. This design enhances durability, lowers manufacturing costs, and eliminates reliance on rare earth materials [4]. The absence of rotor windings also reduces copper losses, further improving efficiency [8].

Various control techniques have been employed to enhance the performance of synchronous reluctance motors [9,10]. Field-Oriented Control (FOC), or vector control, is a leading technique for SynRMs, as it decouples stator current into two orthogonal components: d-axis (responsible for controlling flux) and q-axis (responsible for torque production) [11,12]. This decoupling allows for independent control of torque and flux, resulting in highly efficient and dynamic motor performance. FOC primarily involves applying Clarke and Park transformations to convert three-phase currents into a two-axis (d-q) reference frame, utilizing PID

controllers to regulate d-q currents, and performing inverse transformations to reconstruct three-phase currents for the inverter [12].

Comparatively, Direct Torque Control (DTC) is another advanced control technique for SynRMs that directly regulates torque and flux without a modulator or PWM generator [13-18]. While it provides fast torque response, it suffers from higher torque ripple and less precise flux control than FOC. Its complex switching logic can also introduce harmonics, reducing efficiency [19].

Model Predictive Control (MPC) uses a mathematical model of the SynRM to predict future states and optimize control actions over a finite time horizon [20-22]. While MPC handles nonlinearities and constraints effectively, its computational demands make it less practical for real-time applications compared to the simpler FOC.

Sensorless control techniques, which estimate rotor position and speed without mechanical sensors, offer cost and reliability benefits. Common methods include model-based estimation and high-frequency injection [23]. However, these techniques often require complex algorithms and can struggle with accuracy under varying load conditions, whereas FOC with sensors provides precise control even under dynamic conditions.

Adaptive control adjusts the control parameters in real-time to cope with variations in motor parameters or operating conditions, ensuring robust performance [24,25]. While adaptive control methods like self-tuning regulators and Model Reference Adaptive Control (MRAC) enhance robustness, they add complexity to the system, and their performance is often dependent on the accuracy of the adaptive mechanisms, unlike the well-established and stable performance of FOC.

Sliding Mode Control (SMC) offers robustness to parameter variations and ensures performance under diverse conditions [26]. However, the high-frequency switching characteristic of SMC can lead to chattering, which can be detrimental to the motor and drive system. Modified versions of SMC attempt to mitigate these issues, but they still do not match the balance of performance, ease of implementation, and reliability offered by FOC. Field-Oriented Control (FOC) provides a comprehensive solution for managing synchronous reluctance motors, combining precise torque and flux control with dynamic performance and relative simplicity in implementation.

In this research, a fully integrated fuzzy logic-based Field-Oriented Control strategy is proposed, where FLCs are implemented in both the inner and outer control loops. Unlike previous studies that typically apply FLCs to only one control loop, this comprehensive approach enhances system adaptability and robustness.

Furthermore, conventional FOC strategies, including those incorporating fuzzy logic or sliding mode control (SMC), often rely on decoupling control components to compensate for cross-coupling effects between the d-axis and q-axis currents. In contrast, the proposed method eliminates the need for these decoupling components, simplifying implementation while maintaining high dynamic performance. This aspect has not been addressed in prior research, making the proposed control strategy a novel contribution to the field.

2. MODELLING OF SYNCHRONOUS RELUCTANCE MOTOR

Space vector theory is a powerful mathematical tool used to analyze and control electric machines. It involves the representation of three-phase quantities such as voltages, currents, and magnetic fluxes as two-dimensional vectors in a complex plane as shown in Figure 1. This transformation simplifies the analysis of three-phase systems by converting them into a single vector in the d-q plane (direct-quadrature plane), which corresponds to a rotating reference frame aligned with the rotor's magnetic field [27-28].

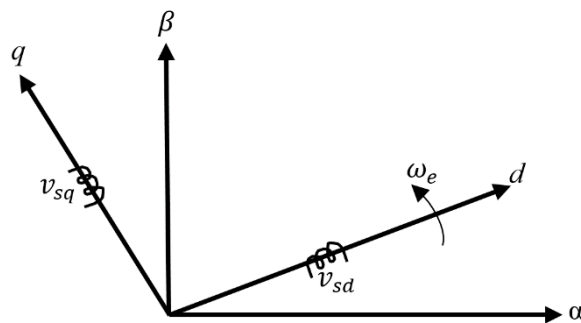


Figure 1. Circuit representation of SynRM

In this study, the SynRM model is derived based on the following assumptions:

- The stator winding is assumed to have a sinusoidal distribution.
- A linear magnetic circuit is considered.
- The rotor has no damper bars.

The motor's space vector model in the synchronously rotating reference frame, which rotates at an electrical angular speed of ω_e , is presented as follows [29-31]:

Voltage Equations:

$$v_{sd} = i_{sd}R_s + \frac{d\psi_{sd}}{dt} - \omega_e\psi_{sq} \quad (1)$$

$$v_{sq} = i_{sq}R_s + \frac{d\psi_{sq}}{dt} + \omega_e\psi_{sd} \quad (2)$$

where

v_{sd} and v_{sq} are the d- and q-axis components of the stator voltage vector, R_s is the stator resistance, i_{sd} and i_{sq} are the d- and q-axis components of stator current vector, ψ_{sd} and ψ_{sq} are the d- and q-axis components of the flux linkage.

Flux Linkage Equations:

The flux linkage vector ψ_s is related to the stator current vector through inductance. For a SynRM, the flux linkage can be formulated as:

$$\psi_{sd} = i_{sd}L_{sd} \quad (3)$$

$$\psi_{sq} = i_{sq}L_{sq} \quad (4)$$

Where, L_{sd} and L_{sq} are the direct and quadrature axis inductances, respectively

Electromagnetic Torque:

The electromagnetic torque produced by the motor along with its dynamic equation of motion is represented as follows:

$$T_e = \frac{3}{2}P(L_{sd} - L_{sq})i_{sd}i_{sq} \quad (5)$$

$$T_e - \beta\omega_r - T_L = J\frac{d\omega_r}{dt} \quad (6)$$

where, ω_r represents the angular mechanical speed, P is the number of pole pairs, T_L is the mechanical load torque, and J is the moment of inertia, β denotes the friction coefficient.

The torque equation can also be expressed as follows

$$T_e = \frac{3}{2}P(\psi_{sd}i_{sq} - \psi_{sq}i_{sd}) \quad (7)$$

3. FIELD-ORIENTED CONTROL STRATEGY OF SynRM

In FOC, the stator currents are decoupled into d-axis (direct) and q-axis (quadrature) components, enabling independent control of magnetic flux and torque similar to a separately excited DC motor. The FOC strategy aligns the stator flux vector with the d-axis ($\psi_{sq} = 0$). From equation (3), it is evident that the direct-axis flux is directly regulated by the d-axis stator current i_{ds} . By substituting $\psi_{sq} = 0$ in equation (7), it will be simplified to

$$T_e = \frac{3}{2}P(\psi_{sd}i_{sq}) \quad (8)$$

Subsequently, from equation (8), it is clear that by maintaining the stator flux constant, the torque can be linearly controlled by the quadrature axis component of the stator current i_{qs} . Therefore, it can be concluded that the FOC strategy achieves decoupled control of speed and flux.

Figure 2 illustrates the schematic diagram of the speed control loop, Figure 3 depicts the schematic diagram for the flux control loop, and Figure 4 presents the overall control system.

In the speed control loop, the reference speed is compared with the actual speed, and the resulting error signal is processed to generate the reference torque. This, in turn, is employed to determine the reference for the q-axis component of the stator current, i_{sq}^* , using equation (8). The command value of i_{sq}^* is subsequently compared with its actual value, and the resulting error signal is controlled to generate the command value of the q-axis stator voltage v_{sq}^* , after adding the decoupling component represented by the third term in equation (2).

In the flux control loop, the command value of the d-axis component of the stator current, i_{sd}^* , is derived from the reference flux using equation (3). This command value is then compared with its actual value,

and the resulting error signal is controlled to generate the reference d-axis component of the stator voltage, v_{sd}^* , after subtracting the decoupling component as indicated by the third term in equation (1).

In this proposed control scheme, the speed control loop typically employs two FLCs to achieve precise and stable operation, while the flux control loop uses only one controller. The speed control loop consists of an outer speed controller and an inner current controller. The outer speed controller regulates the motor speed by generating a torque command, which is then converted into a quadrature-axis current reference (i_{sq}^*). The inner current controller ensures accurate tracking of this reference by generating the quadrature-axis voltage (v_{sq}^*). This cascaded structure is necessary because the outer loop handles slower mechanical dynamics (speed), while the inner loop manages faster electrical dynamics (current), allowing for independent tuning and improved performance.

In contrast, the flux control loop uses a single FLC because flux dynamics are simpler, slower, and decoupled from torque dynamics. A single controller suffices to regulate the direct-axis current (i_{sd}) and maintain the desired flux level, ensuring stable and efficient operation without added complexity.

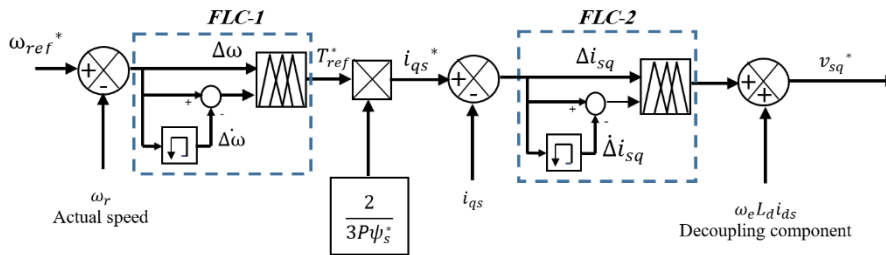


Figure 2. Speed control loop

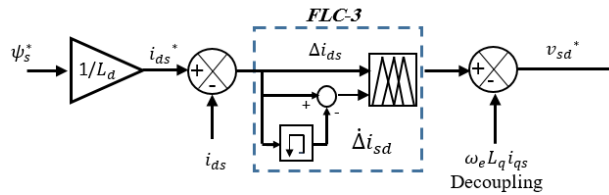


Figure 3. Flux control loop

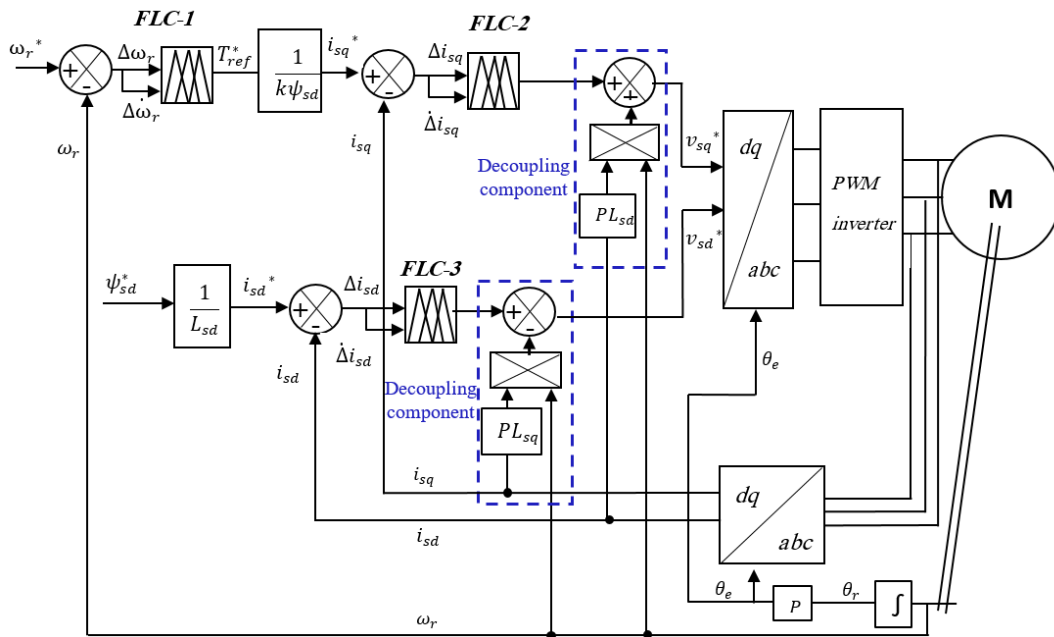


Figure 4. Comprehensive proposed control scheme.

4. FUZZY LOGIC CONTROLLERS

The fuzzy inference system (FIS) used in designing the fuzzy logic controllers, FLC-1, FLC-2, FLC-3, is based on Mandeni's model, as depicted in Figure 5. That FIS comprises of (3) primary components.

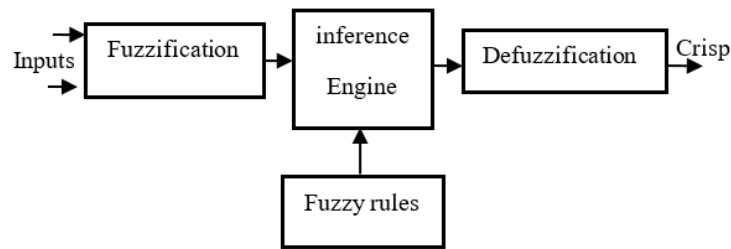


Figure 5. Fuzzy inference system

4.1. Fuzzification process

The fuzzification process is crucial in fuzzy logic systems, allowing them to handle imprecise information. It converts precise input variables into fuzzy inputs for processing within the fuzzy framework. This conversion divides the input variable U into fuzzy sets labeled with terms like "high," "medium," or "low," each defined by a membership function that indicates the degree of membership for each input value.

In the fuzzification process, each precise input (x) is transformed to a fuzzy input by calculating its membership degree μ in each fuzzy set. This degree, ranging from 0 to 1, indicates how well the input aligns with a particular fuzzy set. For instance, as illustrated in Figure 6, a crisp input of -3 might result in a 0.9 membership degree in the "small" fuzzy set, a 0.5 degree in the "medium" set, and 0 in the "large" set. This step is crucial as it provides a foundation for further fuzzy logic operations, allowing for the effective handling and processing of uncertain or imprecise data.

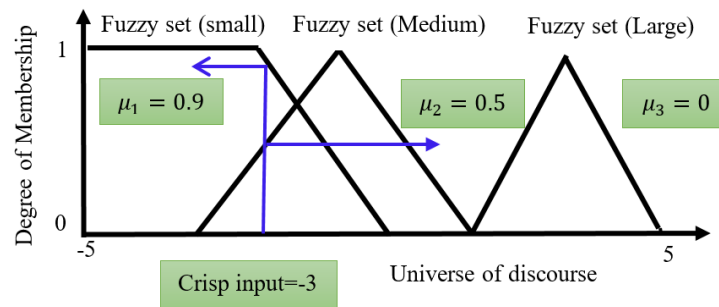


Figure 6. Fuzzification

4.2. Fuzzy rules and operators

Fuzzy logic control systems use a set of "if-then" rules, often based on expert insights, to make decisions in complex, imprecise environments. After inputs are fuzzified into membership values, these values activate corresponding fuzzy rules. For rules with multiple conditions, operators like minimum (AND) or maximum (OR) combine these values into a single output for each rule. The system then aggregates the outputs from all active rules to form a one fuzzy set, called the "aggregated output fuzzy set" as illustrated in Figure 6. This step integrates individual rule outputs into a cohesive fuzzy set, which is then defuzzified to produce a final, precise output.

4.3. Defuzzification process

Defuzzification represents the concluding phase in a fuzzy logic system, where the combined output fuzzy set is converted into a specific, actionable value. This step is critical, as it turns the fuzzy outcomes derived by the system into practical results. Several methods, known as defuzzifiers, facilitate this conversion, with options comprising the centroid method, mean of maximum, bisector, smallest of maximum, and largest of maximum. Each approach offers a different way of deriving a precise value from the fuzzy set to enable a final, usable output.

The centroid method is particularly popular among these techniques. It calculates the crisp output by finding the center of gravity of the area under the aggregated fuzzy set. In essence, the centroid serves as the weighted average of all potential output values, yielding a single value that most accurately reflects the fuzzy set. As depicted in Figure 7, the precise output is situated at the centroid of the fuzzy set, making it a central

point of the aggregated output, which effectively summarizes the overall decision made by the fuzzy logic system.

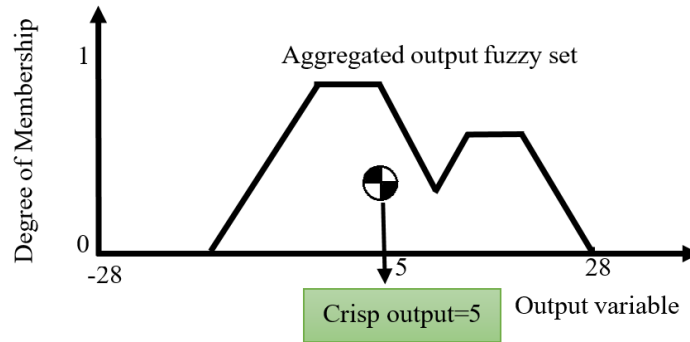


Figure 7. Defuzzification Concept

4.4. Proposed FLCs

The FLC-1 is configured with two input state variables and one output state variable. The first input state variable, the normalized speed error ($\Delta\omega$), includes seven fuzzy sets with linguistic labels: Large positive (LP), Medium positive (MP), and Small positive (SP) zero (Z), Large negative (LN), Medium negative (MN), Small negative (SN) as illustrated in Figure 8-a. The second input state variable, representing the rate of change of speed error ($\Delta\dot{\omega}$), is defined with three fuzzy sets labeled as negative (N), zero (Z), and positive (P), as depicted in Figure 8-b. The output state variable, representing the reference torque change (ΔT^*), is defined by seven fuzzy sets similar to the seven fuzzy sets of ($\Delta\omega$) but with different universe of discourse, as depicted in Figure 8-c.

FLC-2, shown in Figure 9, includes two input and one output state variable. The input state variables for FLC-2 are the normalized error of the q-axis stator current component, Δi_{sq} , and the rate of change of this normalized error, $\Delta \dot{i}_{sq}$.

Similar to FLC-2, FLC-3, depicted in Figure 10, also features two input and one output state variable. Here, the input state variables are the normalized error of the d-axis stator current component, Δi_{sd} , and the rate of change of this normalized error, $\Delta \dot{i}_{sd}$.

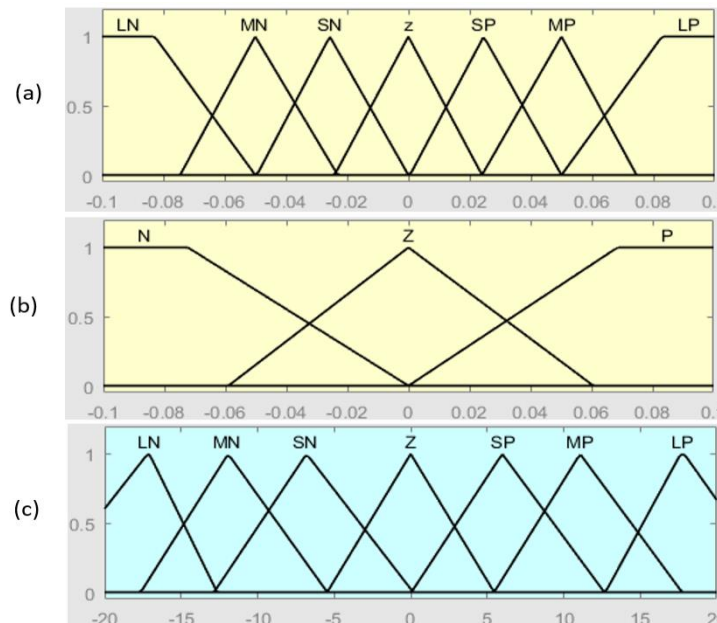


Figure 8. FLC-1, **a**: input speed error $\Delta\omega$, **b**: input rate of change of speed error $\Delta\dot{\omega}$, **c**: output

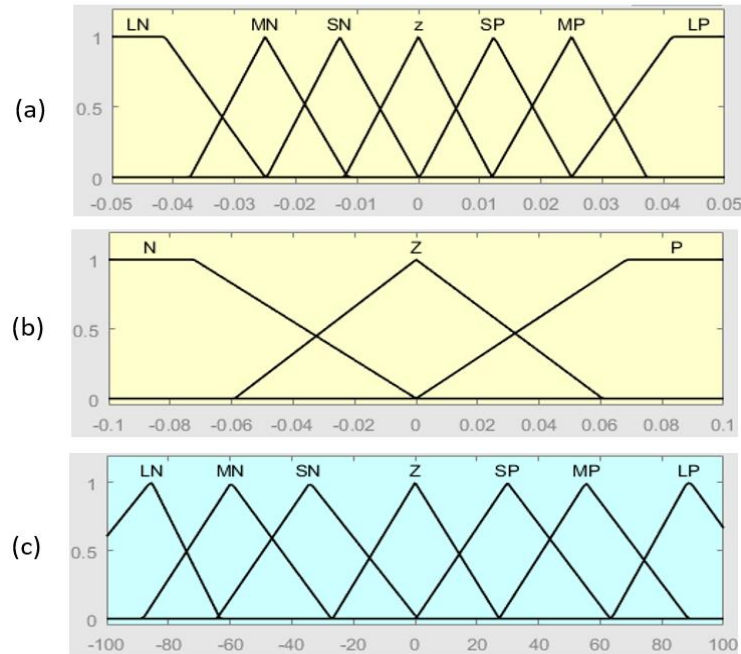


Figure 9. FLC-2, **a:** input q-axis current error Δi_{sq} , **b:** input rate of change of speed error $\Delta \dot{i}_{sq}$, **c:** output

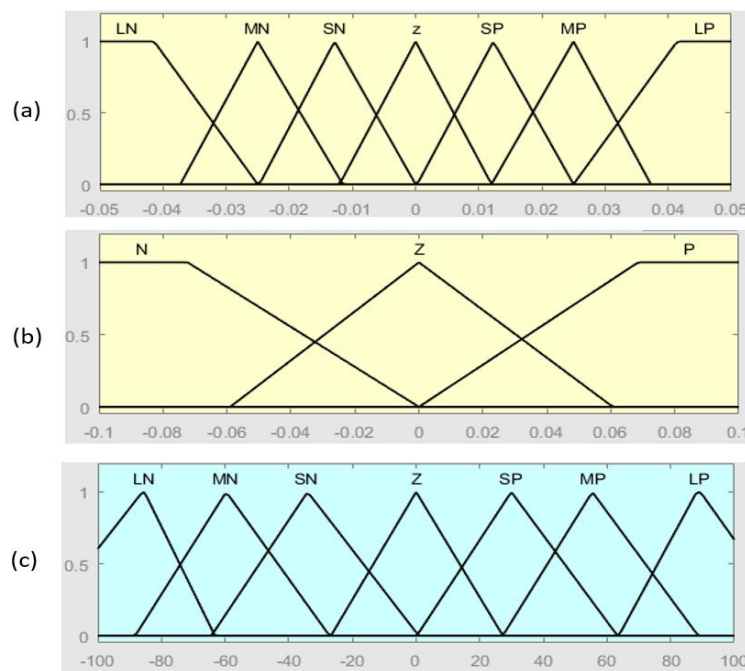


Figure 10. FLC-3, **a:** input q-axis current error Δi_{sd} , **b:** input rate of change of speed error $\Delta \dot{i}_{sd}$, **c:** output

Table 1 outlines the twenty-one fuzzy rules applied in the proposed FLCs, where each rule corresponds to two input membership functions. To evaluate the rule outputs, the minimum (AND) operator is used. The defuzzification process relies on the centroid method. A graphical view of the fuzzy rule surface of FLC-1 is provided in Figure 11.

An illustration of the Fuzzy Inference System (FIS) operation is provided in Figure 12, which depicts the rule viewer of FLC-1. As an example, when the crisp input for the normalized speed error ($\Delta\omega$) is 0.05, it fully activates the fuzzy set Medium Positive (MP) with a membership degree of 1. Simultaneously, if the rate of change of speed error ($\Delta\dot{\omega}$) is -0.02, it partially activates the fuzzy set Negative (N) with a membership degree of 0.25 and the fuzzy set Zero (Z) with a membership degree of 0.75.

During the inference process:

- The input pair (MP & N) activates Rule 13, producing an output fuzzy set MP with a membership degree of 0.25 (determined by minimum (1 & 0.25)).

- The input pair (MP & Z) activates Rule 14, generating an output fuzzy set Large Positive (LP) with a membership degree of 0.75 (minimum (1 & 0.75)).
- Finally, the defuzzification process, using the centroid method, computes a crisp output value of 14.7, demonstrating how the system determines the final control action based on the given fuzzy inputs.

Table 1. Fuzzy Control System Rules

		Speed error						
		LN	MN	SN	Z	SP	MP	LP
Change of speed error	N	LN	LN	LN	Z	MP	MP	LP
	Z	LN	LN	SN	Z	MP	LP	LP
	P	LN	MN	SN	SP	LP	LP	LP

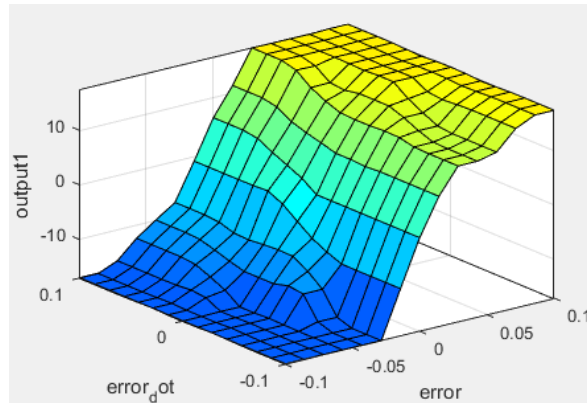


Figure 11. Visualization of the rule surface for the proposed FIS

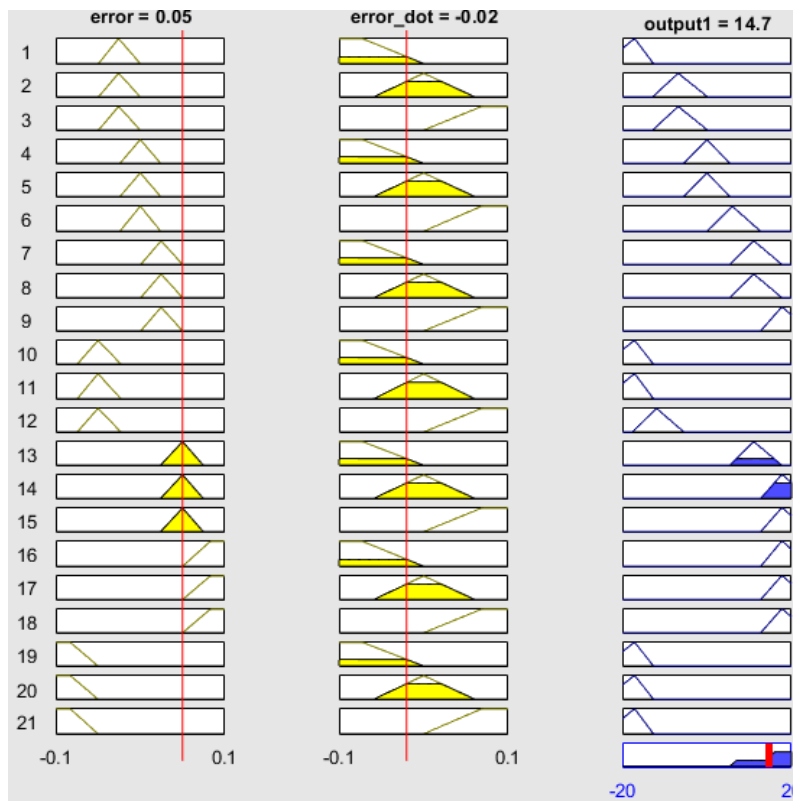


Figure 12. Visualization of the rule viewer for the proposed FLC-1

5. SIMULATION RESULTS

The proposed system shown in Figure 4 is modeled and simulated in MATLAB Simulink with a 50 μ s sampling period, fixed command flux (ψ^*) of 0.9 Wb and inverter DC link voltage (E_{dc}) of 600 V. The numerical values of the motor parameters are presented in Table 2.

Table 2. SynRM Parameters

Rated Power	2.2KW
L_{sd}	0.345H
L_{sq}	0.051H
R_s	2.5 Ω
p	2
J	0.0091Kg.m ²
B	N.m /rad/s

5.1. Evaluation of Dynamic System Performance through Step Changes in Speed Command

The proposed system's performance, as illustrated in Figure 4, is examined using simulations that include successive changes in reference speed while the motor is full loaded. Initially the reference speed set at 1500 rpm. At $t=0.5$ seconds, the reference speed is suddenly decreased from 1500 rpm to 1000 rpm then followed by another sudden decrease at $t=1$ second, bringing the reference speed to 500 rpm.

In Figure 13, the motor speed response shows that it accelerates from rest to 1500 rpm with a rise time of 85 ms and settles within 130 ms. The first peak speed is reached at 131 ms, with only slight overshoot of 5 rpm above the reference speed. As the reference speed drops from 1500 rpm to 1000 rpm at $t=0.5$ seconds, the motor rapidly adapts to the new target, demonstrating a fall time of 25 ms, a settling time of 42 ms, and a peak time of 43 ms. The undershoot is slight, with just a brief increase of 6 rpm below the steady-state value, leading to a 0.6% deviation. In the last adjustment from 1000 rpm to 500 rpm, the response shows a fall time of 24 ms, a settling time of 31 ms, and a peak time of 32 ms. There is a minor undershoot of 8 rpm, leading to a 1.6% deviation from the target speed.

The developed torque of the motor and the load torque are illustrated in Figure 14, demonstrating torque ripples during steady-state operation, with a peak-to-peak amplitude of 5.5 N·m. In Figure 15, the three-phase stator currents under full load conditions reach a magnitude of 5A RMS, and the current waveform frequency decreases as the motor slows.

Finally, Figure 16 illustrates the rotating magnetic flux, showing that the flux maintains a constant amplitude of 0.9 Wb, accompanied by ripples measuring 0.14 Wb.

The proposed system's performance, as illustrated in Figure 4, is examined using simulations that include successive changes in reference speed while the motor is full loaded. Initially the reference speed set at 1500 rpm, at $t=0.5$ seconds, the reference speed is suddenly decreased from 1500 rpm to 1000 rpm then followed by another sudden decrease at $t=1$ second, bringing the reference speed to 500 rpm.

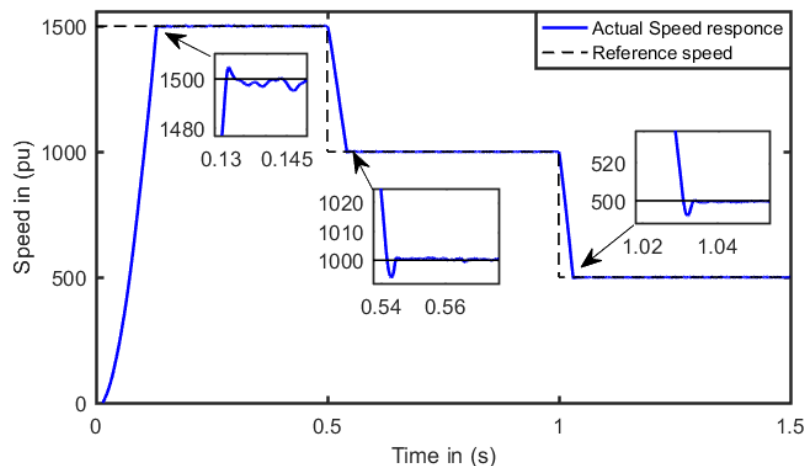


Figure 13. Reference and Actual motor speed

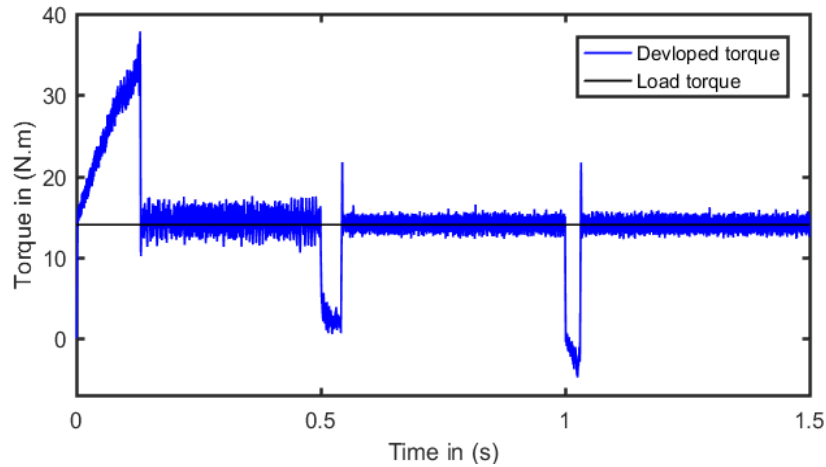


Figure 14. Load torque and motor developed torque

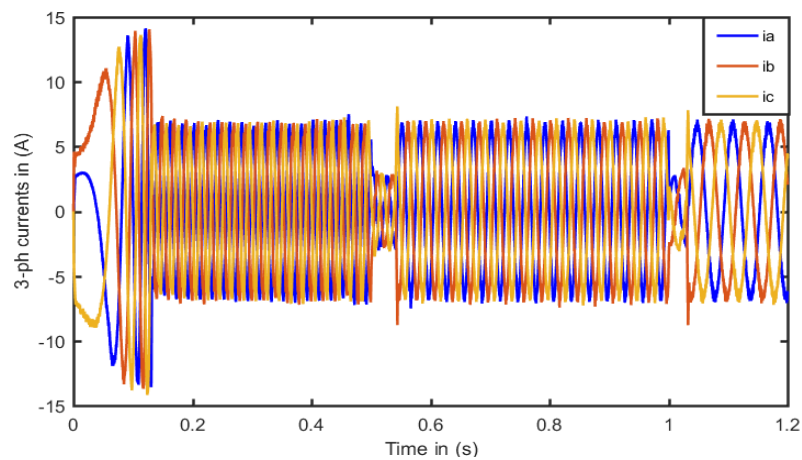


Figure 15. Stator 3-phase currents

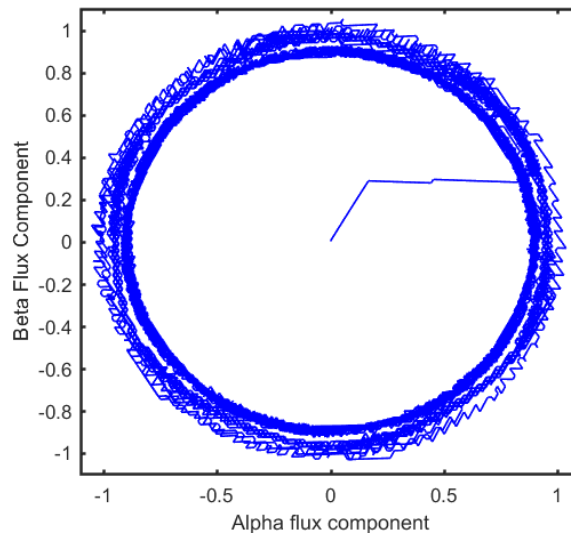


Figure 16. stator rotating flux

5.2. Evaluation of dynamic system performance for a step change of reference speed under different loading conditions.

In this scenario, the system is initiated with a command speed of 1500 rpm at no-load condition. At 0.5s, a full load is abruptly applied, followed by the sudden removal of the load at 1 second. Figure 17 illustrates the motor's dynamic speed response, showcasing its ability to quickly and accurately follow the command

speed. The developed torque corresponding to this response is shown in Figure 18, while Figure 19 depicts the waveforms of the three-phase current.

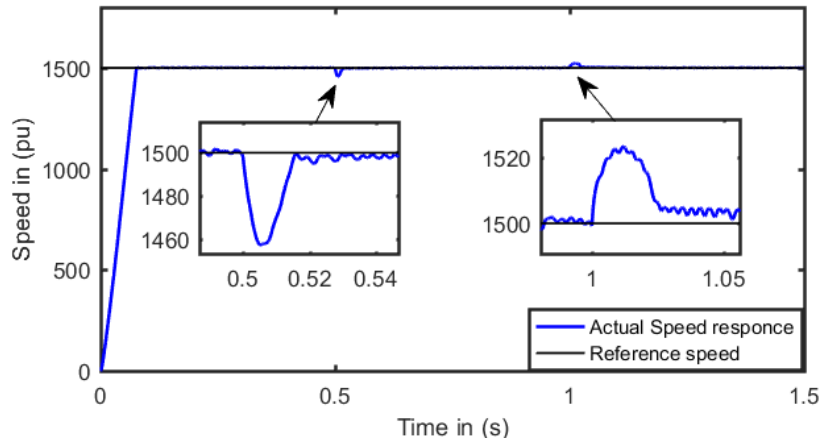


Figure 17. Motor speed response with different loading conditions

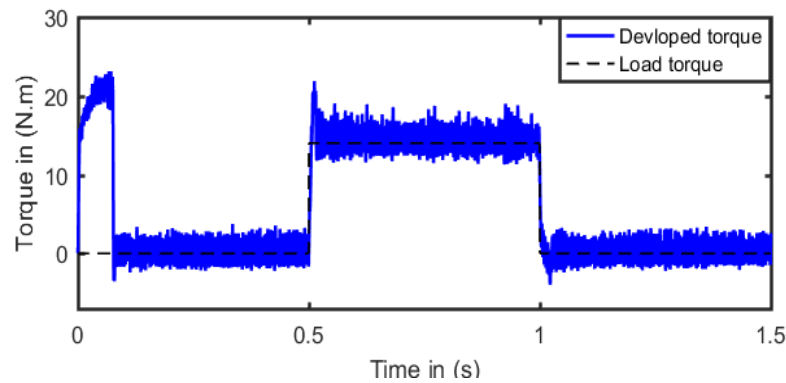


Figure 18. Motor developed torque response with different loading conditions

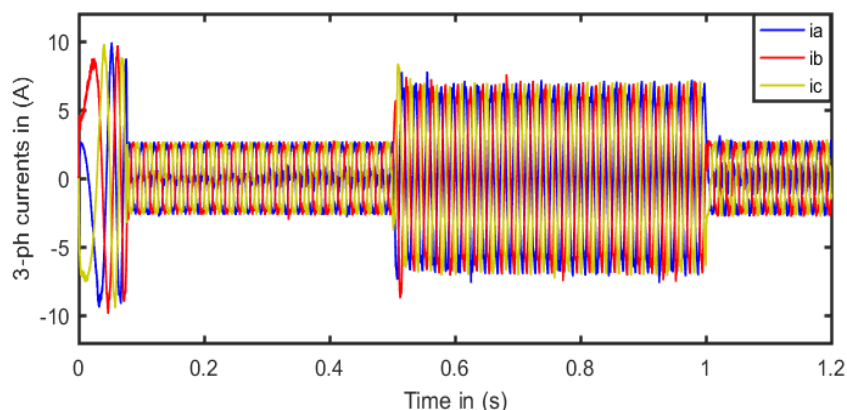


Figure 19. Motor 3-phase currents with different loading conditions

5.3. Evaluation of dynamic system performance without decoupling control components

In this case, the performance of the proposed control system was evaluated under conditions where the decoupling control components were removed, as shown in Figure 20.

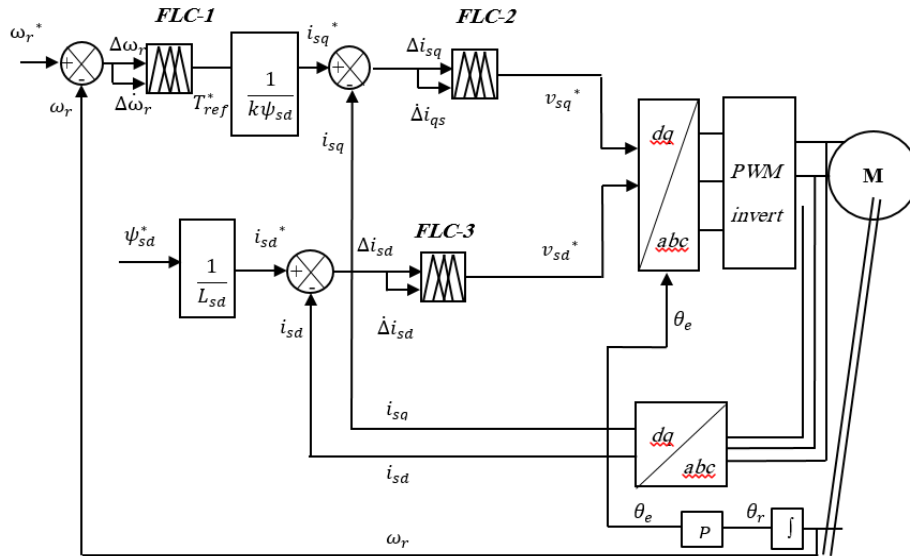


Figure 20. The proposed control algorithm without decoupling control component

Initially, the system was subjected to a sequential step change in speed command. Figure 21 provides a comparative assessment of the speed response with and without decoupling control components. At startup, the system achieves a rise time of 8.5 ms without decoupling components and 9.1 ms with them, while the settling time slightly increases from 12.4 ms to 13.1 ms. The overshoot is measured at 4.5 rpm (0.3%) without decoupling components and 4.7 rpm (0.31%) with them.

For a step-down transition from 1500 rpm to 1000 rpm, the fall time is 3.75 ms without decoupling and 4.2 ms with it, with the undershoot decreasing from 10 rpm (1%) to 6 rpm (0.6%). Likewise, for a step-down from 1000 rpm to 500 rpm, the fall time is 2.9 ms without decoupling and 3.1 ms with it, while the undershoot reduces from 10 rpm (2%) to 8 rpm (1.6%).

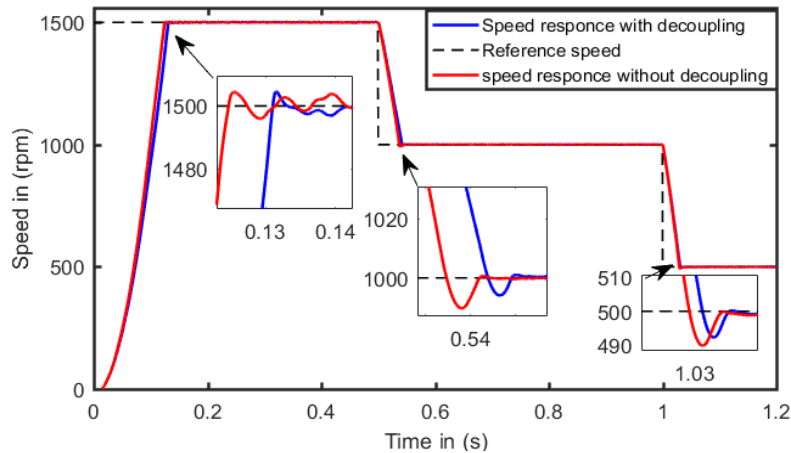


Figure 21. The speed response with and without the decoupling control components

To further evaluate the system performance, a step command speed of 1500 rpm was applied at no load at $t = 0$ s. At $t = 0.5$ s, a full load torque was suddenly introduced, and at $t = 1$ s, the load was abruptly removed. As shown in Figure 22, at startup, the proposed control system exhibits a fast dynamic response, reaching steady-state speed with a rise time of 5.4 ms without the decoupling control component, compared to 5.9 ms with it. The settling time is 7 ms without the decoupling component and 7.6 ms with it.

When the full load is suddenly applied at $t = 0.5$ s, the speed response experiences an undershoot of 52 rpm (3% of the rated speed) without the decoupling control component, whereas with it, the undershoot is reduced to 47 rpm (2.8%). Upon sudden load rejection, the speed overshoot reaches 20.5 rpm (1.3%) without the decoupling component and 23.5 rpm (1.6%) with it.

The analysis demonstrates that removing the decoupling control component enhances rise time, settling time, and overshoot performance, while causing a slight increase in undershoot. This trade-off results

in a faster dynamic response at the expense of minor undershoot degradation. However, a key advantage of eliminating the decoupling components in the proposed control algorithm is the reduced dependency on machine parameters, which improves system robustness and adaptability.

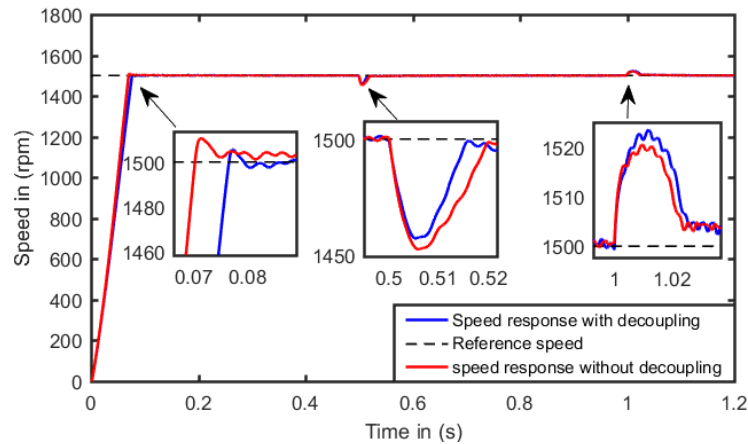


Figure 22. speed response under different loading conditions

6. COMPARING THE PROPOSED FIELD ORIENTED CONTROLLER AND EXISTING FOC STRATEGIES

Field-oriented control (FOC) is a method used widely for motor processes that typically involves PI speed and current controllers for their operation. Although PI controllers are quite simple and effective, they are sensitive to variations of parameters and require extensive tuning. Other methods like Model Reference Adaptive Control (MRAC) and Sliding Mode Control (SMC) provide improved robustness with an increased computational complexity. Fuzzy Logic Controllers (FLCs) have been investigated as another option, which is more accommodating of nonlinearities and uncertainties. The proposed scheme enhances conventional FOC structure by extending the speed control loop with two FLCs: speed control and current control. This feature dramatically improves transient response, robustness, and torque regulation. In contrast to PI-based FOC, this method reduces the dependency on accurate machine parameters and enhances adaptability. And compared to SMC, it avoids chattering and offers improved computational efficiency.

The benefits of the proposed method over the other FOC methods can be summarized as follows:

- Improved Dynamic Response: Faster rise time and better settling time.
- Robustness to Parameter Variations: Reduced sensitivity to machine parameters.
- Decoupled Speed and Torque Control: Precise speed regulation with accurate torque control.
- Computational Efficiency: Enhanced performance without excessive complexity.

This approach provides a more adaptive and efficient motor control solution compared to conventional FOC strategies.

7. PRACTICAL IMPLEMENTATION CHALLENGES AND CONSIDERATIONS

While the proposed fuzzy logic-based Field-Oriented Control (FOC) strategy has been validated through MATLAB/Simulink simulations, real-world implementation introduces additional challenges:

- **Sensor Noise and Measurement Errors:** Speed and current sensors may introduce noise and inaccuracies. Filtering techniques, such as low-pass or Kalman filters, can help improve measurement accuracy.
- **Parameter Variations:** Motor parameters change due to temperature, aging, or tolerances. The proposed FLCs inherently handle uncertainties, but online parameter estimation could further enhance performance.
- **Real-Time Computation Constraints:** Fuzzy logic controllers require real-time computation. DSPs, FPGAs, or microcontrollers with sufficient processing power can ensure efficient execution without affecting control response.
- **Experimental Validation:** Future work will focus on testing the control scheme on hardware to assess its robustness under real conditions, including disturbances and load variations.

Addressing these challenges will enable the proposed FLC-based FOC strategy to be effectively adapted for real-world applications.

8. CONCLUSION

This paper has presented a fuzzy logic controller-based Field-Oriented Control strategy for synchronous reluctance motors to address inherent nonlinearities and parameter sensitivities. Simulation results demonstrate that integrating FLC into the FOC framework significantly enhances dynamic performance by improving rise time, settling time, and torque ripple reduction. Additionally, the proposed approach eliminates decoupling control components, which improves rise time, settling time, and overshoot, with a minor increase in undershoot. This trade-off results in a faster dynamic response while reducing dependency on machine parameters, enhancing system robustness and adaptability. Despite the increased computational demands of FLC, the overall benefits confirm its potential for advanced motor control applications. As the demand for high-performance, reliable electric motors continues to grow, the proposed FLC-based FOC strategy offers a viable solution to meet these objectives.

REFERENCES

- [1] Khaleel, Mohamed, Abdussalam Ali Ahmed, and Abdulagader Alsharif. "Technology challenges and trends of electric motor and drive in electric vehicle." *Int. J. Electr. Eng. and Sustain.* 2023, 41-48.
- [2] Bukhari, Syed Abid Ali Shah, and Vikram Kumar. "Development of a Synchronous Reluctance Motor for Industrial application." *Sukkur IBA Journal of Emerging Technologies*, 2024, 15-23.
- [3] Bezdenezhnykh, Iliia, Vladimir Smirnov, and Viktor Denisenko. "Advantages of Synchronous Reluctance Motors and Synchronous Motors with Permanent Magnets as Drive of Liquid Natural Gas Submerged Pumps for Process Loss Reduction." In *2023 Belarusian-Ural-Siberian Smart Energy Conference (BUSSEC)*, IEEE, 2023, pp. 28-32.
- [4] A. K. and K. Selvajyothi, "Performance Comparison of Synchronous Reluctance Motor and Interior Permanent Magnet Synchronous Motor for Traction Application," *2021 International Aegean Conference on Electrical Machines and Power Electronics (ACEMP) & 2021 International Conference on Optimization of Electrical and Electronic Equipment (OPTIM)*, Brasov, Romania, 2021, pp. 100-106.
- [5] Murataliyev, Mukhammed, Michele Degano, Mauro Di Nardo, Nicola Bianchi, and Chris Gerada. "Synchronous reluctance machines: A comprehensive review and technology comparison." *Proceedings of the IEEE* 110, 2022, 3, 382-399.
- [6] Heidari, Hamidreza, Anton Rassõlkin, Ants Kallaste, Toomas Vaimann, Ekaterina Andriushchenko, Anouar Belahcen, and Dmitry V. Lukichev. 2021. "A Review of Synchronous Reluctance Motor-Drive Advancements" *Sustainability* 13, no. 2: 729.
- [7] Du, Guanghui, Guiyuan Zhang, Hui Li, and Chengshuai Hu. "Comprehensive Comparative Study on Permanent-Magnet-Assisted Synchronous Reluctance Motors and Other Types of Motor" *Applied Sciences*, 2023, 13, no. 14: 8557.
- [8] Tawfiq, Kotb B., Mohamed N. Ibrahim, E. E. El-Kholy, and Peter Sergeant. "Performance improvement of synchronous reluctance machines—a review research." *IEEE Transactions on Magnetics* 57, no. 10 (2021): 1-11.
- [9] Zahraoui, Yassine, Mohamed Moutchou, and Souad Tayane. "Robust vector control of synchronous reluctance motor using space vector modulation algorithm." In *The Proceedings of the International Conference on Smart City Applications*, 2022, pp. 655-665. Cham: Springer International Publishing.
- [10] Gora, Rijul, Riddhiman Biswas, Rahul Kumar Garg, and Uma Nangia. "Field oriented control of permanent magnet synchronous motor (PMSM) driven electric vehicle and its performance analysis." In *2021 IEEE 4th International Conference on Computing, Power and Communication Technologies (GUCON)*, 2021, pp. 1-6.
- [11] Ramesh, P., M. Umavathi, C. Bharatiraja, G. Ramanathan, and Sivaprasad Athikkal. "Development of a PMSM motor field-oriented control algorithm for electrical vehicles." *Materials Today: Proceedings* 65 (2022): 176-187.
- [12] Qinglong, Wang, Yu Changzhou, and Yang Shuying. "Indirect field oriented control technology for asynchronous motor of electric vehicle." In *IEEE International Conference on Power, Intelligent Computing and Systems (ICPICS)*, 2020, pp. 673-677.
- [13] Wang, Ao, Housheng Zhang, Junjie Jiang, Duo Jin, and Shengjie Zhu. "Predictive direct torque control of permanent magnet synchronous motors using deadbeat torque and flux control." *Journal of Power Electronics* 23, no. 2 (2023): 264-273.
- [14] Wu, Xu, Wenxin Huang, Xiaogang Lin, Wen Jiang, Yong Zhao, and Shanfeng Zhu. "Direct torque control for induction motors based on minimum voltage vector error." *IEEE Transactions on Industrial Electronics* 68, no. 5 (2020): 3794-3804.
- [15] Le, Thanh-Lam, and Min-Fu Hsieh. "An enhanced direct torque control strategy with composite controller for permanent magnet synchronous motor." *Asian Journal of Control*, 2024.
- [16] Cai, Jun, Xiaolan Dou, Adrian David Cheok, Ying Yan, and Xin Zhang. "Overview of the Direct Torque Control Strategy in Switched Reluctance Motor Drives." *IEEE Transactions on Transportation Electrification*, 2024.
- [17] Sayed o. madbouly "Torque/Speed Control of 3PH Synchronous Reluctance Motor Using Direct Torque Control" *International Review of Electrical Engineering (IREE)*, August 2022, Vol. 17.
- [18] Sayed o. madbouly "Fuzzy Logic Based DTC Control of Synchronous Reluctance Motor" *Indonesian Journal of Electrical Engineering and Informatics (IJEI)*, 2024, vol. 12.

- [19] Hadla, Hazem, and Fernando Santos. "Performance comparison of field-oriented control, direct torque control, and model-predictive control for SynRMs." *Chinese Journal of Electrical Engineering*, 2022, 8, 24-37.
- [20] Cimini, Gionata, Daniele Bernardini, Stephen Levijoki, and Alberto Bemporad. "Embedded model predictive control with certified real-time optimization for synchronous motors." *IEEE Transactions on Control Systems Technology* 29, no. 2 (2020): 893-900.
- [21] Li, Teng, Xiaodong Sun, Gang Lei, Youguang Guo, Zebin Yang, and Jianguo Zhu. "Finite-control-set model predictive control of permanent magnet synchronous motor drive systems—an overview." *IEEE/CAA Journal of Automatica Sinica* 9, no. 12 (2022): 2087-2105.
- [22] Khalilzadeh, Mohammad, Sadegh Vaez-Zadeh, Jose Rodriguez, and Rasool Heydari. "Model-free predictive control of motor drives and power converters: A review." *IEEE Access*, 2021, 9, 105733-105747.
- [23] Gao, Fengtao, Zhonggang Yin, Pinjia Zhang, Yanqing Zhang, and Yanping Zhang. "A position sensorless control method robust to inductance mismatch for synrm based on generalized multiple model resonant kalman filter." *IEEE Transactions on Power Electronics* 39, 2024, no. 5, 5510-5521.
- [24] Jia, Chao, Wei Qiao, Junwei Cui, and Liyan Qu. "Adaptive model-predictive-control-based real-time energy management of fuel cell hybrid electric vehicles." *IEEE Transactions on Power Electronics* 38, 2022, no. 2, 2681-2694.
- [25] Wu, Jian, Junda Zhang, Baochang Nie, Yahui Liu, and Xiangkun He. "Adaptive control of PMSM servo system for steering-by-wire system with disturbances observation." *IEEE Transactions on Transportation Electrification* 8, 2021, no. 2, 2015-2028.
- [26] Shimamoto, Keita, and Toshiyuki Murakami. "Position and Cross-Coupling Factors Estimation for Sliding Mode Current Control Based Position-Sensorless Control of IPMSM." *IEEE Access* 2022, 10, 74873-74882.
- [27] Fadul, Saber ME, Ishak Aris, Norhisam Misron, Izhal A. Halin, and AKM Parvez Iqbal. "Modelling and simulation of electric drive vehicle based on Space Vector Modulation technique and Field Oriented Control strategy." In *2017 International Conference on Communication, Control, Computing and Electronics Engineering (ICCCCEE)*, 2017, pp. 1-7.
- [28] BETZ, Robert E., and M. G. Jovanović. "Introduction to the space vector modeling of the brushless doubly fed reluctance machine." *Electric Power Components and Systems* 31, 2003, no. 8, 729-755.
- [29] Yamamoto, Shu, Takuya Kojima, and Hideaki Hirahara. "Mathematical Models of Synchronous Reluctance Motor Considering Iron Loss and Cross-Magnetic Saturation with Reciprocity Relation of Mutual Inductance." *IEEJ Journal of Industry Applications* 11, 2022, no. 1, 206-215.
- [30] Sriprang, Songklod, Nitchamon Poonnoy, Babak Nahid-Mobarakeh, Nouredine Takorabet, Nicu Bizon, Pongsiri Mungporn, and Phatiphat Thounthong. "Design, Modeling, and Model-Free Control of Permanent Magnet-Assisted Synchronous Reluctance Motor for e-Vehicle Applications." *Sustainability* 14, 2022, no. 9, 5423.
- [31] Accetta, Angelo, Maurizio Cirrincione, Marcello Pucci, and Antonino Sferlazza. "Space-vector state dynamic model of the synchronous reluctance motor considering self, cross-saturation and iron losses." In *2021 IEEE Energy Conversion Congress and Exposition (ECCE)*, 2021, pp. 4164-4170.

BIOGRAPHY OF AUTHORS



Sayed O. Madbouly received the B.Sc., M.Sc., and Ph.D. degrees in Electrical Engineering from Ain Shams University, Egypt, in 1998, 2004, and 2010 respectively. From 2010 to 2013, he is an Assistant Professor in the Electrical Power and Machines Department, Faculty of Engineering, Ain Shams University, Egypt. Since 2013, he is an Assistant Professor in the Electrical Engineering Department, College of Engineering, Qassim University, Saudi Arabia. His major research interests include electrical machines, renewable energy, and control of electrical machines.

E-mails: so.ossman@qu.edu.sa & sayed_madpouly@hotmail.com